Cortico-Muscular Coherence with Time Lag with Application to Delay Estimation

Yuhang Xu, Verity M. McClelland, Zoran Cvetković, and Kerry R. Mills

***Abstract*—Functional coupling between the motor cortex and muscle activity is usually detected and characterised using the spectral method of cortico-muscular coherence (CMC). This functional coupling occurs with a time delay which, if not properly accounted for, may decrease the coherence and make the synchrony difficult to detect. In this paper we introduce the concept of cortico-muscular coherence with time lag (CMCTL), that is the coherence between segments of motor cortex electroencephalogram (EEG) and electromyography (EMG) signals displaced from a central observation point. This concept is motivated by the need to compensate for the unknown delay between coupled cortex and muscle processes. We demonstrate using simulated data that under certain conditions the time lag between EEG and EMG segments at points of local maxima of CMCTL corresponds to the average delay along the involved cortico-muscular conduction pathways. Using neurophysiological data, we then show that CMCTL with appropriate time lag enhances the coherence between cortical and muscle signals, and that time lags which correspond to local maxima of CMCTL provide estimates of delays involved in cortico-muscular coupling that are consistent with the underlying physiology.**

***Index Terms*—Cortico-muscular coherence (CMC), electroencephalogram (EEG), electromyogram (EMG), motor control system, global time delay.**

I. Introduction

THE spectral technique of cortico-muscular coherence (CMC) has become one of the primary methods for quantifying functional coupling between the motor cortex and muscle activity [2]–[6] since Conway found the initial evidence in humans of significant coherence between the motor cortex electroencephalogram (EEG) and the surface electromyogram (EMG) of the first dorsal interosseous (FDI) muscle during constant isometric contractions [7]. EEG and EMG events that are coherent do not occur simultaneously, but with a time delay which reflects signal propagation time between the brain and the muscle and possible information processing. If not accounted for, this delay may decrease the level of coherence [8], and thus make the cortico-muscular coupling difficult or impossible to detect. In this paper we propose a cortico-muscular coherence with time lag (CMCTL) function, that is the coherence between segments of motor cortex EEG and EMG signals displaced from a central observation point, and show that it enhances the level of CMC and provides a more detailed information about the temporal structure of cortico-muscular interactions than the conventional CMC. Then we propose an algorithm for the estimation of the delay between coherent EEG and EMG events. The algorithm amounts to finding the the time lag which maximises local coherence. In addition to its relevance to enhancing the CMC, knowing the time delay between the motor cortex and the periphery can reveal important information about the communication between motor cortex and muscles by characterising the direction via which the oscillations propagate and/or by differentiating the cortico-spinal pathways via which the activity is transmitted. This is important not only for increasing our fundamental understanding of the physiology of cortex-muscle interations, but also for increasing the potential utility of cortico-muscular coherence as a clinical and research tool.

A method which is widely used for identification of time delays in biological systems is based on the estimation of the slope of the phase of the cross spectral density of considered processes [9]–[12]. This approach has however produced conflicting results [3], [13]–[15] and also suffers from some methodological problems. In particular, the slope of the cross spectral density is well defined only if the two processes are connected via a linear-phase system, which is in general not satisfied by cortico-muscular pathways. This issue has been addressed by Lindemann *et al.* [11] who proposed using the Hilbert transform to identify and remove the phase component which is not linear and then estimate the delay from the remaining linear component. Unfortunately, their work has rarely been used in physiological studies, which could be due to its technical sophistication and underlying assumptions which are difficult to verify in practice. Further, there is evidence of bidirectional connectivity in the motor control system [15]–[17] and the delay estimated from phase spectrum is subject to errors if the coupling is bidirectional in the estimated period [18], [19]. Although some groups have considered directed coherence based on the Granger causality [15], [20]–[22] which in principle can discern different propagation directions, the results vary much from individual to individual. Moreover, there could be more than one event in the observation period and the delay of each event could be different. Finally, many groups perform EMG rectification prior to calculation of CMC, which introduces nonlinear distortion of the EMG signal, including its phase spectrum [23].

The concept of delay estimation via the time offset that maximises coherence of two signals has been previously applied successfully to acoustic signals [24]. It has also been used in

This work was presented in part at ICASSP 2016 [1].

Yuhang Xu and Zoran Cvetković are with the Department of Informatics, King's College London, The Strand, London WC2R 2LS, UK (e-mail: {yuhang.xu; zoran.cvetkovic}@kcl.ac.uk)

Verity M. McClelland and Kerry R. Mills are with the Academic Unit of Clinical Neurophysiology, King's College Hospital, Denmark Hill, London SE5 9RS, UK (email: verity@betterley.co.uk; prof.krmills@mac.com)

the context of cortico-muscular interactions, but with a limited success [25] and under the assumption of continuous constant-delay flow of information in narrow frequency bands, which may not be applicable to biological signals such as EEG and EMG [25]. The authors conclude that further work is needed to make the method applicable to non-stationary events. We revisit the concept and introduce a series of modifications that make it yield delay estimates consistent with underlying physiology. More importantly, we study the interpretation of the results provided by the method in the context of multi-path propagation, which is a more realistic model of the channels of cortico-muscular communications.

The paper is organised as follows. In Section II, we introduce a model of motor control system, review relevant aspects of coherence analysis, and principles of the delay estimation based on the analysis of the phase spectrum of EEG-EMG cross spectral density. In Section III, we introduce the cortico-muscular coherence with time lag (CMCTL) and the method for the delay estimation. Section IV presents examples of CMCTL applied to physiological data and results of delay estimation. Finally, Section V draws some conclusions.

II. Background

A. Simplified Model of Motor Control System

Cortical events propagate to the periphery and motor cortex also receives input from the periphery [2], [5], [17]. Let us consider first a scenario in which the information transmission is unidirectional, from the cortex to the periphery. This transmission is not instantaneous, but with a delay, which reflects at least neural conduction time. Cortical activity is transmitted to the motoneurones within the spinal cord via the corticospinal tract, which contains nerve fibres of differing conduction velocities. Therefore, each of them may introduce a different delay and attenuation. Each motorneurone innervates multiple fibres within the muscle, comprising a motor unit. The response $y_i(t)$ of a motor unit i can thus be represented as a linear combination of delayed and attenuated versions of the cortical signal $x(t)$, that is $y_i(t) = \sum_{k=0}^{K_i} \alpha_{i,k} x(t - T_i - \tau_{i,k})$, where $a_{i,k}$ are attenuations, while T_i and $\tau_{i,k}$ are delays of individual nerve fibres, defined so that T_i is equal to the minimal delay within the motor unit and $0 = \tau_{i,0} \leq \tau_{i,1} \leq \ldots \leq \tau_{i,K_i}$. Within the pick up area of an electrode, there are several motor units that would be recruited by the same cortical activity [26]–[29]. Therefore, surface EMG (sEMG) signal $y(t)$ is a linear combination of several motor unit signals, as well as signals unrelated to the considered cortical activity, which we will collectively refer to as noise. Surface EMG signal thus has the form $y(t) = \sum_{i=1}^{I} \beta_i y_i(t) + n(t)$, where β_i factors represent the attenuation of the pathways between particular motor units and the electrode, while $n(t)$ is the noise. Expressed in terms of the cortical event $x(t)$ the surface EMG signal therefore has the form

$$y(t) = \sum_{i=1}^{I} \sum_{k=1}^{K_i} \beta_i \alpha_{i,k} x(t - T_i - \tau_{i,k}) + n(t) \ , \qquad (1)$$

that is, $y(t)$ is a sum of delayed and amplitude-scaled versions of $x(t)$. To simplify the notation, in the following we will express the above model as

$$y(t) = \sum_{i=1}^{N} b_i x(t - D_i) + n(t) \ . \qquad (2)$$

One can introduce more complex models of individual fibres, and the propagation between motor units and the electrode, but as long as all stages along the path are modelled as linear filters, the overall system between the cortex and the sEMG electrode will be a causal, finite-impulse-response, linear time-invariant system, the most general form of which is given by (2). Under excitations of small amplitude and within limited time intervals many biological systems can be well approximated by linear time-invariant systems. Besides, coherence analysis applies only to processes connected via linear-time invariant systems, hence our model is not any more restrictive than the fundamental assumptions of coherence analysis.

An analogous model can be established for transmission of sensory events from the periphery. Hence in the case of bidirectional signalling sEMG signal has the form

$$y(t) = y_0(t) + \sum_{i=1}^{N_x} b_{x,i} x_0(t - D_{x,i}) + n_y(t) \ , \qquad (3)$$

while the EEG signal has the form

$$x(t) = x_0(t) + \sum_{i=1}^{N_y} b_{y,i} y_0(t - D_{y,i}) + n_x(t) \ , \qquad (4)$$

where $x_0(t)$ is the cortical event that performs muscle control, whereas $y_0(t)$ is the sensory event which is transmitted to the cortex, while $n_x(t)$ and $n_y(t)$ are noise components.

B. Coherence Analysis

Cortico-muscular coupling is commonly detected and quantified by means of coherence analysis. Coherence $C_{xy}(\omega)$ between two stationary processes $x(t)$ and $y(t)$ is defined as $C_{xy}(\omega) = |S_{xy}(\omega)|^2 / \left(S_{xx}(\omega) S_{yy}(\omega)\right)$ where $S_{xx}(\omega)$ and $S_{yy}(\omega)$ are their power spectral densities, and $S_{xy}(\omega)$ is their cross spectral density [30].

The coherence between non-stationary processes is estimated via the short-time Fourier transform (STFT) [31], which segments signals into intervals over which their statistical properties remain fairly constant. To that end, a window of finite duration T is placed at a discrete set of time instants, $t_c = n\Delta t, \ n \in \mathbb{Z}$, and for each window position, the discrete Fourier transform of the windowed signal is computed at frequencies $\omega_c = 0, \Delta\omega, \ldots, (M-1)\,\Delta\omega, \ \Delta\omega = \frac{\Omega_s}{M}$ where Ω_s is the sampling frequency, and M is the size of the discrete Fourier transform. In this manner time-frequency representations $X(t_c, \omega_c)$ and $Y(t_c, \omega_c)$ are obtained, where $X(t_c, \omega_c)$ and $Y(t_c, \omega_c)$ reflect events within the time-frequency support of the window centred around (t_c, ω_c). In neurophysiological studies, the STFT is typically estimated using windows of length $T = 500$ ms, with shifts Δt between 250 ms and 500 ms. Some transient events, however, are much shorter and could be easily obscured by such short-time Fourier analysis as it reflects cumulative effects of all events within the

window. Shorter windows would therefore be more suitable for the analysis of transient phenomena. However, a better time resolution comes at the expense of a worse frequency resolution, and it is important to ensure that the bandwidth of the window does not exceed considerably the frequency range of interest.

Effects of time-frequency resolution trade-offs in CMC analysis are illustrated in Fig. 1 using EEG and EMG signals collected during a controlled motor task (see Section IV). Signals are sampled at 1024 Hz. The STFT used for the CMC plot in Fig. 1(a) is computed using Hanning window of length $T = 500$ ms (512 samples), at $M = 512$ frequencies, corresponding to $\Delta\omega = 2$ Hz, and with $\Delta t = 250$ ms (256 samples). The coherence plot in Fig. 1(b) is obtained using the same STFT parameters, except that in attempt to refine the time resolution of the analysis Δt is reduced to $\Delta t = 9.8$ ms (10 samples). For the CMC analysis plotted in Fig. 1(c), the STFT is computed using Hanning window of length $T = 125$ ms (128 samples), whereas the time shift is kept at $\Delta t = 9.8$ ms. The coherence plot in this figure suggests that communication between the brain and the muscle involves a sequence of transient events, which on the plots in Fig. 1(a) and Fig. 1(b), corresponding to the 500 ms analysis window, are merged into what appears to be one longer event, even when the shift between consecutive analysis windows is decreased to $\Delta t = 9.8$ ms. The effect of reducing the length of the analysis window further is illustrated in Fig. 1(d), which shows the CMC plot obtained using Hanning window of length $T = 62.5$ ms (64 samples), with $\Delta t = 9.8$ ms. The time-frequency resolution of the STFT in this case does not match well that of the cortico-muscular signals, which results in lower coherence levels, in addition to poor frequency resolution. Fig. 1(e) shows the CMC plot of the same events with spectral estimation performed in the wavelet-transform domain. Morlet wavelet centred at 24 Hz is used, to capture the frequency band of the highest coherence. One can observe that the wavelet analysis due to its low time resolution at low frequencies fails to capture significant coherence patterns below 10 Hz.

Once adequate time-frequency resolution of spectral analysis is decided upon, the time varying power spectra and cross-spectral densities are estimated by averaging the STFT magnitude spectra over different epochs (trials): $\hat{S}_{xx}(t_c, \omega_c) = \frac{1}{L}\sum_{n=1}^{L} |X_n(t_c, \omega_c)|^2$, and analogously for $\hat{S}_{yy}(t_c, \omega_c)$, while $\hat{S}_{xy}(t_c, \omega_c) = \frac{1}{L}\sum_{n=1}^{L} X_n(t_c, \omega_c) Y_n^*(t_c, \omega_c)$, where L is the number of epochs. Therefore, the coherence between $x(t)$ and $y(t)$ is estimated as $C_{xy}(t_c, \omega_c) = |\hat{S}_{xy}(t_c, \omega_c)|^2 / \left(\hat{S}_{xx}(t_c, \omega_c)\hat{S}_{yy}(t_c, \omega_c)\right)$. Significant coherence can be defined by setting the 95% confidence limit (CL) which is estimated as $CL_{(a\%)} = 1 - \left(1 - \frac{\alpha}{100}\right)^{\frac{1}{(L-1)}}$ where α is set to 95 and L is again the number of trials used in the estimation of auto- and cross-spectra [32].

The value of coherence is between zero and one. There are several factors that could make CMC so small that the synchrony between EEG and EMG would be difficult to detect. One of the factors is the noise components, which include not only the environmental noise but also the components unrelated to the process of interest [23]. Another factor is the time delay between synchronised events in the brain and the muscle which can be described as the bias due to misalignment. The effect of misalignment is best illustrated in the case of two processes $x(t)$ and $y(t)$, one of which is a

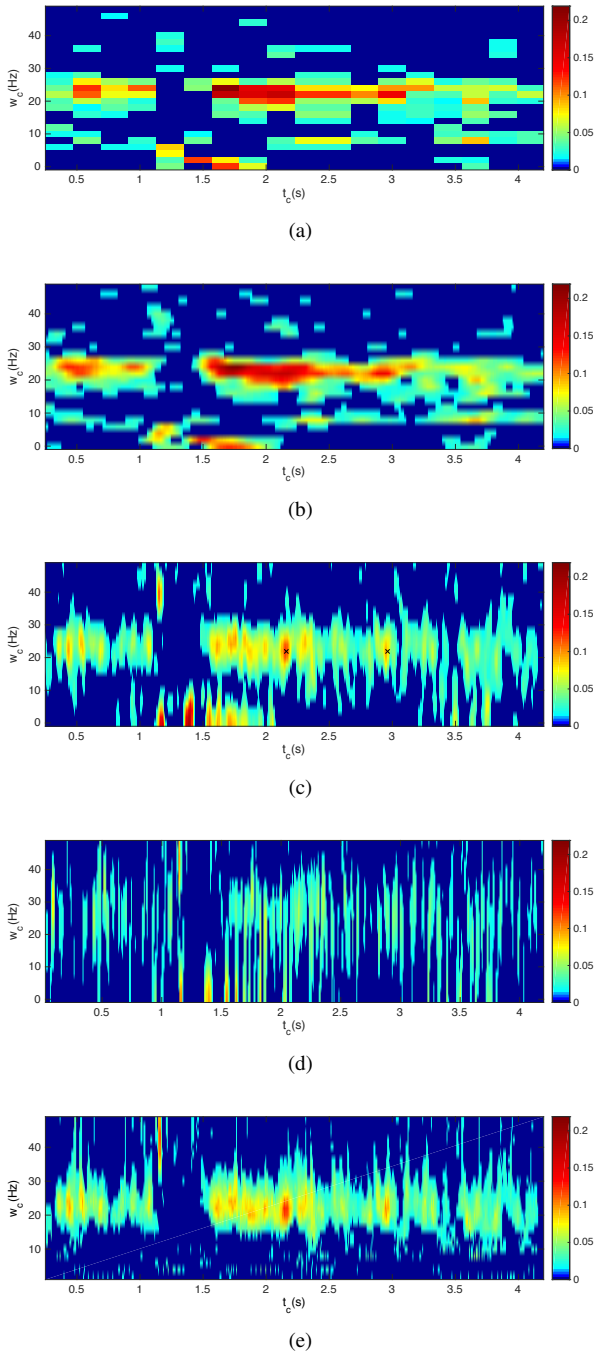

Fig. 1. CMC plots obtained with different time-frequency resolutions of spectral estimation, illustrating its effect on the information revealed by the subsequent coherence analysis. The STFT is computed at $M = 512$ frequencies using Hanning windows of different lengths T and with different shifts Δt between consecutive windows. CMC values below the 95% confidence limit are set to zero. (a) $T = 500$ ms, $\Delta t = 250$. (b) $T = 500$ ms, $\Delta t = 9.8$ ms. (c) $T = 125$ ms, $\Delta t = 9.8$ ms; two most prominent peaks, marked by $\times$ signs, will be referred to in Section IV. (d) $T = 62.5$ ms, $\Delta t = 9.8$ ms. (e) Wavelet coherence using Morlet wavelet centred at 24 Hz.

delayed version of the other,

$$y(t) = bx(t - D) + n(t) \ , \tag{5}$$

where $n(t)$ is additive noise. If the coherence is estimated within an observation window of duration T, the coherence is decreased by a factor, which depends on the ratio between the delay and the duration of the observation window [8], specifically

$$E[\hat{C}(\omega)] \approx \left(1 - \frac{|D|}{T}\right)^2 C_{max}(\omega), \qquad |D| \leq T \tag{6}$$

where $E[\hat{C}(\omega)]$ is the estimated coherence and $C_{max}(\omega)$ is the maximum coherence without misalignment. The estimated coherence would be maximal when there is no time lag. This dependence of coherence level on temporal alignment of considered processes motivates the CMCTL analysis and the delay estimation methodology studied in the next section.

C. Estimation of time delay

The traditional way of time delay estimation is based on the phase model [3], [9]–[15]. The cross-spectrum $S_{xy}(\omega)$ is complex valued and can be expressed in the polar form as $S_{xy}(\omega) = |S_{xy}(\omega)|e^{j\phi_{xy}(\omega)}$ where $\phi_{xy}(\omega)$ is the phase angle between the two processes. If $y(t)$ is a delayed and amplitude-scaled version of $x(t)$, $y(t) = bx(t - D)$, the phase follows a straight line given by the equation $\phi_{xy}(\omega) = \phi_{xy}(0) - \omega D$. Under this model of cortico-muscular signalling pathways, several regression methods have been used so far [33], [34] to estimate the delay between the two processes as the slope of the phase spectrum.

In the traditional procedures, the phase estimate is taken in one or several periods that altogether last for a few seconds, during which a numbers of events could occur. There are several pieces of evidence showing that not only cortex could lead muscle, but also muscle could lead cortex in some circumstances [15], [35], [36]. Thus if the connection between two processes contains components of opposite directions, the phase spectrum represents a complex combination of both. On a more fundamental level, phase estimates can be used when the system follows the single-path propagation model. However, the cortico-muscular conduction system, as modelled in (2) is not a linear-phase system, and moreover, since cortical events propagate to muscles via multiple paths, each of which might introduce a different delay, the question that naturally arises is whether this delay is actually well defined, and if so, what it would be, and how to estimate it. These problems are addressed in the next section.

III. Methods

A. Cortico-Muscular Coherence with Time Lag

Towards achieving time alignment between EEG and EMG events, we propose to consider coherence between their versions shifted in time, in particular we propose the following cortico-muscular coherence with time lag (CMCTL) function

$$C_{xy}(t_c, \tau_1, \tau_2, \omega) = \frac{|\hat{S}_{xy}(t_c + \tau_1, t_c + \tau_2, \omega)|^2}{\hat{S}_{xx}(t_c + \tau_1, \omega)\hat{S}_{yy}(t_c + \tau_2, \omega)} \tag{7}$$

where t_c is the reference observation time instant, while τ_1 and τ_2 are displacements of $x(t)$ and $y(t)$ observations, respectively, from that reference point. Hence, the observation windows for $x(t)$ and $y(t)$ are centred at $t_c + \tau_1$ and $t_c + \tau_2$, respectively. In this manner the compensated time delay between these two processes is $\tau = \tau_2 - \tau_1$.

There are several points regarding CMCTL worth noting:

- Cortico-muscular processes are not stationary and often involve transient events which could be much shorter than the window of the underlying short-time Fourier analysis. Consequently, the fact that two pairs of displacements (τ_1, τ_2) and (τ_1', τ_2') satisfy $\tau_2 - \tau_1 = \tau_2' - \tau_1'$ does not imply that $C_{xy}(t_c, \tau_1, \tau_2, \omega) = C_{xy}(t_c, \tau_1', \tau_2', \omega)$.
- Apparently, one of CMCTL time variables, t_c, τ_1, and τ_2, is redundant, however, having all of them feature explicitly makes the CMCTL function easier to read.
- A convenient way to visualise the CMCTL function is by plotting it in the (τ_1, τ_2) plane for a pair of fixed (t_c, ω_c) parameters. Fig. 2(a) shows an example of the conventional CMC plot with two prominent peaks marked by $\times$ signs, while Fig. 2(b) shows the CMCTL plotted for fixed $t_c = 3.441$ s and $\omega_c = 24$ Hz which are coordinates of the second prominent peak (we consider here the second peak just as an illustration, whereas both peaks are discussed in Section IV). The sampling frequency of data acquisition is $\Omega_s = 1024$ Hz, while the STFT is evaluated at $N = 128$ frequencies using the $T = 125$ ms Hanning window (128 samples). Each point on this plot thus reflects events situated within the corresponding 125 ms interval, and within the 11 Hz frequency band (the bandwidth of the window) centred around 24 Hz.
- Whereas t_c is not explicitly represented on CMCTL plots centred around a fixed (t_c, ω_c) pair, it evolves along the line $\tau_1 = \tau_2$. Hence, the conventional CMC is given by a sequence of regular samples of CMCTL along this line.

Fig. 2 illustrates benefits of the CMCTL compared to the conventional CMC, it terms of either enhancing the coherence or providing additional insights. In particular:

- The coherence maxima do not occur along the line $\tau_1 = \tau_2$, but are seen at points away from this line.
- All local coherence peaks are on the same side of the line $\tau_1 = \tau_2$, suggesting signalling in the same direction; this information is absent from the conventional CMC.
- The duration of cortico-muscular coupling events is always longer if considered along the line of their maximal coherence as opposed to the the line $\tau_1 = \tau_2$.

B. Delay Estimation

According to the formula for the coherence bias in (6), in the case of a single-path system the CMCTL is maximised when the time lag $\tau = \tau_2 - \tau_1$ is equal to the delay between the two processes. However, cortico-muscular interactions involve signalling over multiple paths, as modelled in (2), which blurs the notion of the delay. We propose to introduce the notion of the *global delay*, D_g, and in analogy with the single-path case define it as the time lag between the two processes

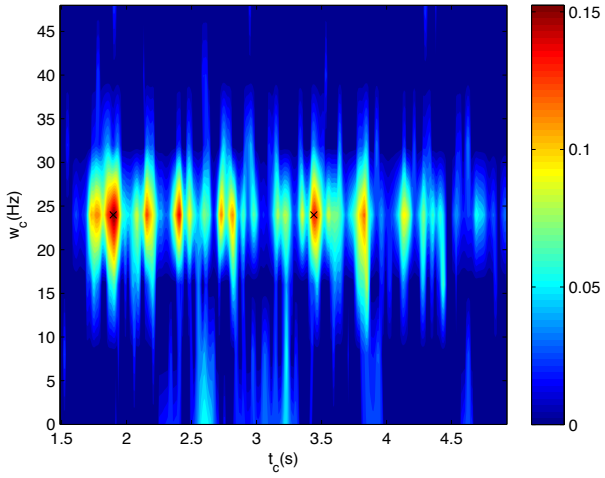

(a)

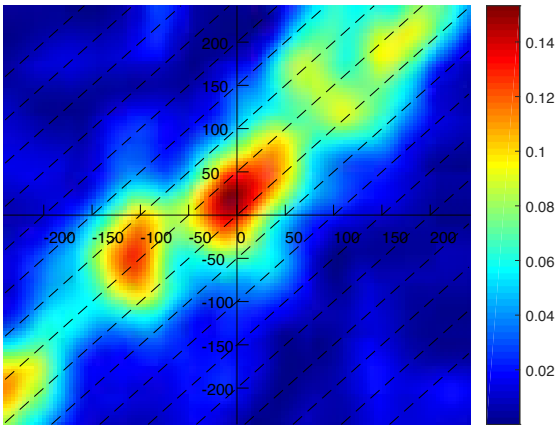

(b)

Fig. 2. Examples the conventional CMC and CMCTL. (a) The conventional CMC for a controlled motor tasks with two prominent coherence peaks marked by $\times$ signs, which will be referred to in Section IV. (b) CMCTL plotted around fixed (t_c, ω_c), in this case the coordinates of the second prominent peak. In this plot the x-axis represents τ_1 and the y-axis represents τ_2 in samples. Note that local maxima of the CMCTL are found away from the $\tau_1 = \tau_2$ line, demonstrating coherence enhancement achieved via CMCTL. Observe also that all local maxima of the CMCTL are situated on the same side of the $\tau_1 = \tau_2$ line, suggesting signalling in one direction.

corresponding to a local maximum of $C_{xy}(t_c, \tau_1, \tau_2, \omega)$:

$$D_g := \tau_2^* - \tau_1^* \ , \ (\tau_1^*, \tau_2^*) = \arg\max_{\tau_1, \tau_2} C_{xy}(t_c, \tau_1, \tau_2, \omega) \ . \quad (8)$$

We will illustrate in the following that under some reasonable assumption the global delay coincides with the mean of the distribution of the delays in the multi-path system.

The CMCTL is a four-dimensional function which is difficult visualise and unnecessary to compute over the full range of its variables t_c, τ_1, τ_2, and ω. We found it practical to first compute the conventional CMC, identify peaks in the (t_c, ω_c) plane, and then compute CMCTL for t_c and ω_c corresponding to the locations of the peaks. Fig. 2 illustrates the procedure. The top plot shows the conventional CMC,

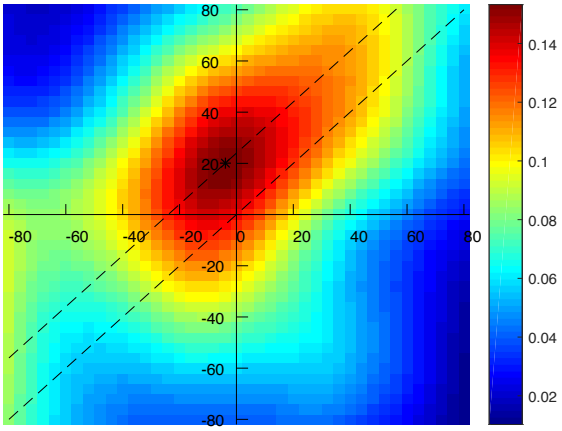

Fig. 3. The procedure of time delay estimation. Here we see the CMCTL plot from Fig. 2(b) at a finer scale. Again, the x-axis represents τ_1 and the y-axis represents τ_2 in samples. The dashed line through the origin corresponds to $\tau_1 = \tau_2$ and the asterisk marks the local maximum of the coherence. The dashed line going through this local maximum, with the slope equal to one intersects the axes at coordinates which are equal to the estimated delay.

where two prominent peaks are identified. The bottom plot then shows the CMCTL centred around the peak at $t_c = 3.441$ s, $\omega_c = 24$ Hz. Fig. 3 then shows the same CMCTL at a finer scale. Displacement pairs (τ_1, τ_2) with the same delay are situated along the lines parallel to $\tau_1 = \tau_2$, while the corresponding delay is equal to the coordinate of the crossing of such lines with the τ_2 axis (or the τ_1 axis, but with the reversed sign of the delay). We can read from the plot in Fig. 3 that the estimated delay is approximately 25 ms.

The concept of the estimation of the delay between two processes via the time lag that maximises their coherence has been previously proposed in the context of cortico-muscular coherence by Govindan *et al.* [25]. The authors proposed it for the estimation of the delay between stationary narrow-band signals, which inherently involves spectral estimation over relatively long time segments, and assumes constant-delay flow of information from one process to the other. The authors conclude that these assumptions are frequently violated in biological systems and that further work is needed to address the dynamic nature of cortico-muscular interactions. Our method is designed to specifically deal with non-stationary processes, by using much shorter analysis windows (an order of magnitude shorter), which consequently cover a broader range of frequencies, and performing the estimation around local peaks of the CMC in the time-frequency plane. Further, due to the assumed stationarity, in [25] the authors estimate the delay by considering only time lags along τ_1 and τ_2 axes, whereas we consider the CMCTL in the whole (τ_1, τ_2) plane, and we will see in Section IV that the maximum is always found away from the axes. Another major methodological difference is that in [25] the authors propose rectification of EMG signals, which we avoid due to its non-linear nature and the resulting modification of the spectral content of EMG signals [23]. As a result of all these modifications we obtain

delay estimates which are in much closer agreement with underlying physiology (see Section IV). Finally, we provide an interpretation of delay estimates in the context of multi-path propagation, and that is discussed in the next subsection.

C. Physical Interpretation of the Global Delay

According to (6), which is derived for two processes $x(t)$ and $y(t)$ such that $y(t) = bx(t-D) + n(t)$, if in order to compensate for the delay we shift $y(t)$ by D_s in the opposite direction, the bias ratio of the coherence becomes

$$\frac{E[\hat{C}(\omega)] - C_{max}(\omega)}{C_{max}(\omega)} \approx -\frac{2|D-D_s|}{T} + \left(\frac{|D-D_s|}{T}\right)^2 \quad (9)$$

Apparently, the coherence would be maximal when D_s is equal to the delay. However, if we consider the model of motor control system in (2), surface EMG signal has the form $y(t) = \sum_{i=1}^{N} b_i x(t-D_i)+n(t)$, which is a sum of several delayed and amplitude-scaled versions of the EEG signal $x(t)$ and additive noise. If we introduce a shift D_s in $y(t)$, the sEMG signal becomes $y(t+D_s) = \sum_{i=1}^{N} b_i x(t-D_i+D_s) + n(t)$, hence

$$\begin{aligned} S_{xy}(\omega) &= E\left[\frac{1}{T}X(\omega)Y^*(\omega)\right] \\ &= \frac{1}{T}\int_0^T\int_0^T E\Big(x(v)\big(\sum_{i=1}^{N} b_i x^*(u-D_i+D_s) + n^*(u)\big)\Big) \\ &\quad \times e^{-j\omega v}e^{j\omega u}dudv \\ &= \frac{1}{T}\int_0^T\int_0^T \big(\sum_{i=1}^{N} b_i R_{xx}(u-v-D_i+D_s)e^{j\omega(u-v)}\big)dudv \quad (10) \end{aligned}$$

where R_{xx} is the autocorrelation function of $x(t)$. By letting $g = u - v$ and assuming R_{xx} is narrow, we obtain that

$$\begin{aligned} S_{xy}(\omega) &= \frac{1}{T}\big(\sum_{i=1}^{N} b_i \int_{-T}^{T}(T-|g|)R_{xx}(g-D_i+D_s)e^{j\omega g}dg\big) \\ &\approx \left(\sum_{i=1}^{N} b_i\big(1-\frac{|D_i-D_s|}{T}\big)e^{j\omega(D_i-D_s)}\right)S_{xx}(\omega) \quad (11) \end{aligned}$$

In such a scenario, where the output is a sum of several delayed versions of the input, we cannot compensate all involved delays $D_1, D_2, ..., D_N$, but we can just find D_g which maximises the coherence. The bias ratio between the coherence and its maximum in this case has the following form

$$\frac{E[\hat{C}(\omega)]-C_{max}(\omega)}{C_{max}(\omega)} \approx \frac{\left|\sum_{i=1}^{N} b_i\big(1-\frac{|D_i-D_s|}{T}\big)e^{j\omega D_i}\right|^2}{\left|\sum_{i=1}^{N} b_i\big(1-\frac{|D_i-D_g|}{T}\big)e^{j\omega D_i}\right|^2} - 1 \quad (12)$$

It can be shown that the same expression is valid also for the more general model described by (3) and (4) under the following two assumptions: (i) concurrent sensory and cortical events $x_0(t)$ and $y_0(t)$ are uncorrelated, (ii) $S_{x_0,x_0}(\omega) \approx S_{y_0,y_0}(\omega)$. The first assumption amounts to the fact that the brain cannot respond instantaneously to sensory input, while the second would be satisfied if both R_{x_0,x_0} and R_{y_0,y_0} are narrow so that their spectra are approximately flat. The difference in the the bias ratio formula in (12) between the unidirectional and bidirectional signalling scenarios is in that delays D_i take only positive values in the former case, whereas in the latter case they can have both positive and negative values. Finding an analytical solution for the time lag D_g which maximises the coherence seems very challenging. Below we simulate such a multi-path system and investigate the impact of parameters of the distribution of the delays on D_g and the drop-off of the coherence away from its maximum.

The physiological data which we use in this study pertain to movement control of the hand, so in simulations of (12) we will set parameters to reflect signal propagation between the cortex and hand muscles. The scale factors and delays in the above models are influenced by several factors which include conduction velocity, fibre length, fibre diameter etc. [37], [38]. Based on the conduction velocity values of the nerve fibres, which is around $50-65$ m/s in the arms [39]–[41], and setting the distance between the scalp and the hand to around 1.2 m, we obtain that most of the delays D_i are between 18 ms to 24 ms. To introduce the effects of other factors, such as the conduction velocities of other kinds of fibres and the differences of their lengths, in the first instance we will assume that D_i follow Gaussian distribution with mean of 20 ms and standard deviation of 4 ms, which means about 95% of the delays are between 12 ms and 28 ms. It has long been held that the surface myoelectric activity assumes a Gaussian amplitude distribution [42]–[46], hence we will draw attenuation parameters b_i also according to a Gaussian distribution normalised between 0.05 and 0.95.

Fig. 4 shows results of simulations of the multi-path formula in (12) for different propagation scenarios. The curve corresponding to the single-path bias formula in (9) is represented by the dashed blue line, as a reference case where the delay is unambiguously defined. In Fig. 4(a) we show first the case when D_i have Gaussian distribution with mean 20 ms and standard deviation 4 ms. The global delay D_g which maximises the coherence is in this case equal to the mean delay and the coherence has a relatively sharp peak at this value of D_g. We obtained almost identical plots for D_i distributed according to the mixture of three Gaussians, with means at 15 ms, 20 ms, and 25 ms, with equal standard deviations of 4 ms, and weights equal to 0.25, 0.5 and 0.25 respectively. Fig. 4(b) illustrates the case when each path involves also several branches. In particular, we simulate explicitly the model in (1), which considers T_i and $\tau_{i,k}$ separately. We show the cases when T_i have Gaussian distribution with mean 20 ms and standard deviation 4 ms, while $\tau_{i,k}$ have Gaussian distribution with different means and different standard deviations. This case also represents a model which involves linear time-invariant filtering along each path. In Fig. 4(b), the global delay of each case is the sum of the means of T_i and $\tau_{i,k}$, that is again the overall mean propagation time.

Finally we investigate effects of bidirectional signalling during the observation window. Fig. 5(a) shows the scenario in which one quarter of D_i are reversed, that is D_i is distributed according to a mixture of two Gaussians, one with mean -20 ms and the other with mean 20 ms, both with the same

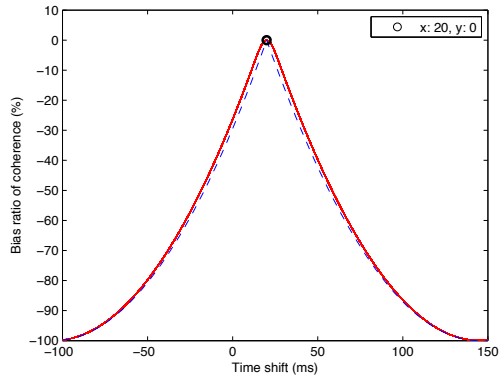

(a)

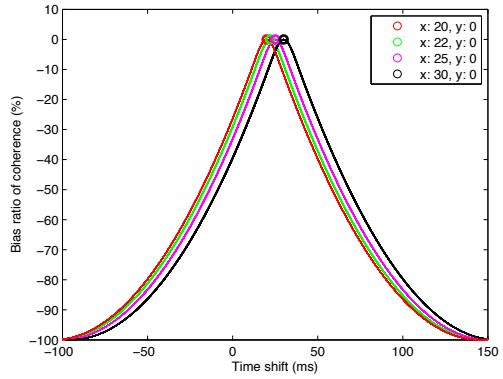

(b)

Fig. 4. Coherence bias curves in (12) for different distributions of delays between the brain and the muscle, along with the curve corresponding to the single-path case in (9) (dashed-blue). Each solid curve consists of 1000 curves, each of which is a different simulation of (12). The delay in the reference equation (9) is set to be the same as the corresponding global delay D_g of (12). (a) D_i assume Gaussian distribution with mean of 20 ms and standard deviation of 4 ms. (b) The delays are modelled according to (1), where T_i assume Gaussian distribution with mean of 20 ms and standard deviation of 4 ms, while for $\tau_{i,k}$ four cases are considered: $\tau_{i,k}$ are all set to zero (red), which gives again the curves plotted in (a), and then $\tau_{i,k}$ assume Gaussian distributions with mean of 2 ms and standard deviation of 1 ms (green), mean of 5 ms and standard deviation of 1 ms (pink), and mean of 10 ms and standard deviation of 2 ms (black). The frequency f is set to 24 Hz and T is set to 125 ms. In all considered cases, coherence bias curves have maxima at time shifts D_g which coincide with means of propagation delay distributions.

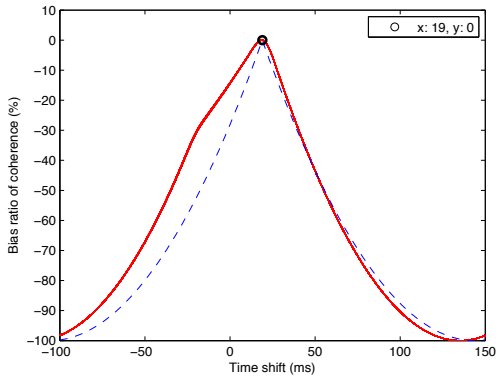

(a)

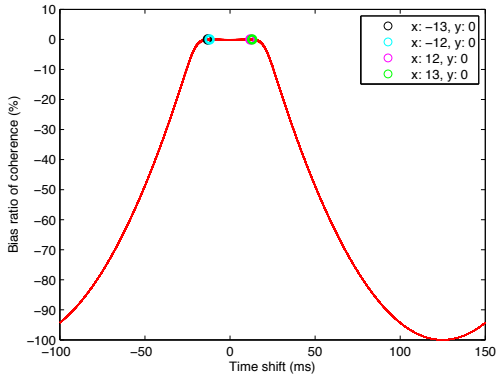

(b)

Fig. 5. Coherence bias curves in (12) for bidirectional coupling scenarios. (a) D_i are distributed according to a mixture of two Gaussians with standard deviation of 4 ms, and means of 20 ms and -20 ms, with weights equal to 0.75 and 0.25, respectively. Coherence bias curves in this case have prominent peaks, but their locations yield underestimates of mean delays of propagation in the dominant direction. Note, however, that although as much as 25% of signalling propagates in the opposite direction, the estimate of the mean delay in the dominant direction is not far from the actual value, *i.e.* 19 ms as opposed to 20 ms. (b) D_i are distributed according to a mixture of two Gaussians with standard deviation of 4 ms and means of 20 ms and -20, ms with equal weights. In this case there is no dominant direction of propagation. Coherence bias curves exhibit multiple local maxima, as marked on the plot, but these are not prominent. Instead, the curves exhibit a plateau which extends between the means of delays in the two directions. In all simulations, the frequency f is set to 24 Hz and T is set to 125 ms.

standard deviation of 4 ms, and with weights equal to 0.25 and 0.75, respectively. The value of D_g is now 19 ms, which is slightly smaller than the mean value of the delays in the dominant direction of propagation. The other example is an extreme situation illustrated in Fig. 5(b), corresponding to the mixture of the same two Gaussians but with equal weights. Whereas there are now four local maxima of the coherence, at D_g equal to -13 ms, -12 ms, 12 ms or 13 ms, they are not prominent, and in fact the most prominent feature of the curve is its plateau which extends from -20 ms to 20 ms.

IV. Experimental Results

A. Signal Acquisition

The proposed methodologies were applied to data collected from healthy subjects in an experiment designed to investigate the modulation of cortico-muscular coherence by peripheral stimuli [47].

Subjects sat comfortably at a table and performed a simple motor task with their right hand, holding a 15 cm plastic ruler in a key grip between the thumb and index finger, keeping the ruler parallel to and 2 cm above the table surface. Mechanical perturbations to the motor task were provided from an electromechanical tapper that generated pulses of lateral displacement of the ruler, giving the subjects the sensation that their grip on the ruler may be lost. The subjects were asked to hold the ruler gently against the stylus of the tapper to maintain its position as well as they could throughout each run. A single trial lasted 5 seconds, with the stimulus delivered 1.1 s after the start of the data collection period. The stimuli were delivered at pseudorandom intervals varying between 5.6 s and

8.4 s (mean 7 s) so that subjects could not anticipate the arrival of the next stimulus. Up to 200 epochs of data were collected for each subject. EMG was recorded using adhesive electrodes in a belly-tendon montage over first dorsal interosseous (FDI) of the dominant hand. Bipolar EEG was recorded from the scalp overlying the contralateral motor cortex. EMG and EEG signals were amplified and bandpass filtered (0.5 - 100 Hz for EEG; 5 - 500 Hz for EMG). Raw EEG signals were scrutinized off-line by eye and any epochs of data containing movement artefacts were rejected from further analysis [47].

For the original neurophysiology study [47], we recruited 12 healthy subjects. The coherence observed in a majority of subjects was however very weak. One such instance of weak coherence is illustrated in Fig. 9. It can be noted that except in a short interval immediately following the stimulus, the coherence is weak and, moreover, the time-frequency region where the CMC is present is very sparse. For the development and validation of the methodology presented in this study, we therefore considered 5 subjects with pronounced coherence patterns, such as the one illustrated in Fig. 1.

B. Time-Frequency Analysis

Signals collected in the experiment were analysed using the short-time Fourier and wavelet transforms with time-frequency resolutions described in Section II-B, as illustrated in Fig. 1 for signals corresponding to subject J. The STFT using Hanning window of length $T = 125$ ms, with time shifts of $\Delta t = 9.8$ ms between consecutive analysis windows (Fig. 1(c)) provided the most suitable time-frequency resolution in terms of being able to discriminate between consecutive transient events without a considerable drop in coherence levels and it will be used in all experiments reported in this section. Fig. 1(c) shows most pronounced coherence in the frequency band centred at 24 Hz, and two prominent coherence peaks, which will refer to as Peak 1 and Peak 2. With the other four subjects, we also observed two prominent coherence peaks (see Fig. 2 for data of Subject B). Centre frequencies, time instants, and levels of prominent coherence peaks of each subject are shown in Table I. It can be noticed that the first prominent peak always appears between 1.5 s and 2.5 s while the second one appears between 2.5 s and 3.5 s.

C. Delay Estimation and Coherence Enhancement

After the two most prominent peaks are identified, we considered the CMCTL at time instants t_c and frequencies ω_c corresponding to these peaks. Delay parameters τ_1 and τ_2 were varied in increments of 4 samples points (about 3.9 ms) each. Before presenting results of delay estimation, it is of interest to investigate the drop-off of CMCTL away from local maxima. To that end we fixed τ_1 at the value corresponding to a local maximum of CMCTL and varied τ_2. Fig. 6 shows the drop-off curves obtained in this manner for both prominent peaks for two subjects. The drop-off curves corresponding to Peak 2 both subjects are close to the drop-off profiles in Fig. 4 that correspond to unidirectional propagation, whereas the drop-off curves corresponding to Peak 1 are much wider, resembling more scenarios with bidirectional signalling illustrated in Fig. 5. A possible explanation is that Peak 1 is situated within a short time interval following the mechanical stimulus, when there could be more pronounced bidirectional signalling before movement control stabilises.

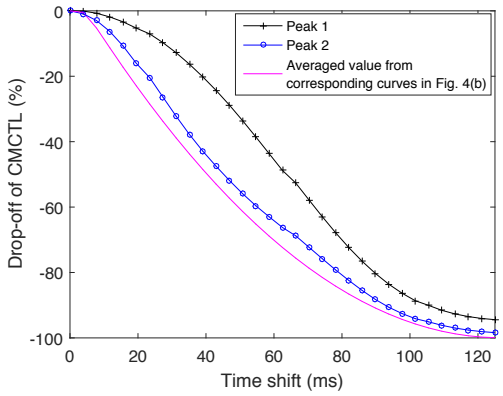

(a)

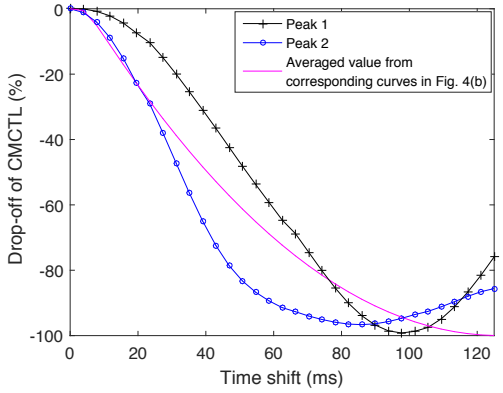

(b)

Fig. 6. Comparison between the bias ratio of Peak 1 (black), Peak 2 (blue) and the averaged values from the curves in Fig. 4(b) (pink). (a) Subject K (b) Subject L. The curves around Peak 2 are close to the drop-off profiles in Fig. 4(b) (pink), which correspond to unidirectional propagation, whereas the drop-off curves around Peak 1 are much wider, resembling more scenarios with bidirectional signalling illustrated in Fig. 5.

Fig. 7 shows the CMCTL around Peak 1 for two subjects (J and N). We can observe from these plots and the data in Table II that the CMCTL practically does not change in the small neighbourhood of the origin $(\tau_1, \tau_2) = (0, 0)$, which based on the analysis in Section III-C and simulations shown in Fig. 5 suggests bidirectional signalling, and hence delay estimates that are lower than actual delays. It can be also noticed in Fig. 7(c) that there are areas of CMCTL increase on both sides of the $\tau_1 = \tau_2$ line, supporting further the presence of signalling in both directions. Fig. 7(b)(d) shows at a finer scale CMCTL regions around their local maxima, which are marked by "$*$". The intersection of the dashed-line passing though the coherence maximum with the τ_2 line in Fig. 7(b)(d) then gives an estimate of the corresponding delays. Fig. 8 shows the CMCTL around Peak 2 for the same two subjects. It is evident from the figure and data in Table II that now the CMCTL increases significantly away from the origin $(\tau_1, \tau_2) = (0, 0)$, and also that the highest coherence is found on the same side

TABLE I
LOCATIONS OF THE PROMINENT PEAKS OF THE CMC ACROSS SUBJECTS.

Subject	Peak 1			Peak 2		
	Time (s)	Value	Frequency (Hz)	Time (s)	Value	Frequency (Hz)
B	1.898	0.1575	24	3.441	0.1356	24
J	2.162	0.1107	24	2.963	0.0842	24
K	1.674	0.1856	24	2.689	0.1490	24
L	2.123	0.0897	16	2.680	0.0771	16
N	1.957	0.0839	16	3.256	0.0578	32

TABLE II
ESTIMATES OF GLOBAL TIME DELAYS AND LEVELS OF CMCTL INCREASE AT LOCAL MAXIMA COMPARED TO THE ORIGIN.

Subject	Peak 1		Peak 2	
	Global time delay (ms)	Coherence increase (%)	Global time delay (ms)	Coherence increase (%)
B	23.4 $\pm$3.9	4.88	23.4 $\pm$3.9	13.01
J	15.6 $\pm$3.9	1.86	23.4 $\pm$3.9	19.51
K	7.8 $\pm$3.9	2.00	15.6 $\pm$3.9	4.39
L	11.7 $\pm$3.9	5.58	19.5 $\pm$3.9	8.20
N	-11.7 $\pm$3.9	2.72	15.6 $\pm$3.9	19.45

of the line $\tau_1 = \tau_2$, suggesting signalling in one direction and more accurate and reliable delay estimates. The global time delays estimated in this manner around Peak 1 and Peak 2 for the five subjects are shown in Table II (recall that the time resolution of the CMCTL used for delay estimation is 3.9 ms). All delays estimated around Peak 2 are in the region 19.5 ± 3.9 ms which agrees with physiological facts discussed earlier. Delay estimates around Peak 1 are on average smaller, but still within the 19.5 ± 3.9 ms region except for Subject K. These lower delay estimates could be attributed to bidirectional signalling.

Next we compare the above delay estimates to those obtained using the linear phase model approach [9], its variation which estimates the non-linear component of the phase using the Hilbert transform [11], and the existing method based on maximising coherence [25]. Following the argument presented in [9], we applied a weighted least squares regression in the frequency range of significant coherence to fit a straight line through the phase of the cross-spectral density between EEG and EMG signals. Only data collected in post-stimulus periods from 1.5 s to 4.5 s were used. These recordings were divided into three 1 s long non-overlapping segments. The time delays obtained in this manner vary widely across subjects. In order to decrease the effects caused by the non-stationarity of the signals and make the comparison with our algorithm more direct, we applied the phase method to different time intervals separately too. Then we applied the modified algorithm based on the Hilbert transform. Finally, we used the existing method based on maximising coherence. Table III shows the estimated time delays in different intervals with these three approaches. Note that delays shorter than 10 ms are physiologically impossible given conduction velocities in nerve fibres [48]. Our results in Table II are most directly comparable to the results of the other three methods in the $1.5 - 2.5$ s and $2.5 - 3.5$ s ranges as Peak 1 and Peak 2 which are selected to estimate the global time delay around are located in these intervals for all the subjects. Comparing Table II with Table III, shows that results of our method are both more mutually consistent and in closer agreement with the underlying physiology.

D. Further Considerations

Physiological studies have found that around $10 - 25\%$ of healthy subjects do not express significant cortico-muscular coherence. A question that naturally arises is whether in such cases the CMCTL can enhance the cortico-muscular coherence to a level above significance threshold. As we pointed out in Section II-B, there are two known factors that could make CMC fall below the significance threshold: one is the bias due to misalignment, and the other is the contamination of EEG and EMG signals with noise and processes which are unrelated to the monitored activity [23]. The CMCTL methodology can compensate the bias due to misalignment, and in some cases that would be sufficient to reveal coherence which is normally not expressed. However, CMCTL cannot remove noise and other irrelevant EEG and EMG components, and if their combined level is high enough compared to the process of interest, the CMCTL alone will not be able to bring the coherence above significance threshold. Whereas we are presently investigating de-noising techniques, it is worth noting that adequate time-frequency resolution of spectral estimation which precedes coherence evaluation has the capability of implicitly enhancing the ratio between relevant signals and noise. To observe the underlying mechanism, note that the STFT transform is a two-dimensional sequence of correlations between a signal of interest and time-frequency atoms $\phi_{t_c,\omega_c}(t) = w(t - t_c)e^{j\omega_c t}$, where $w(t)$ is the STFT

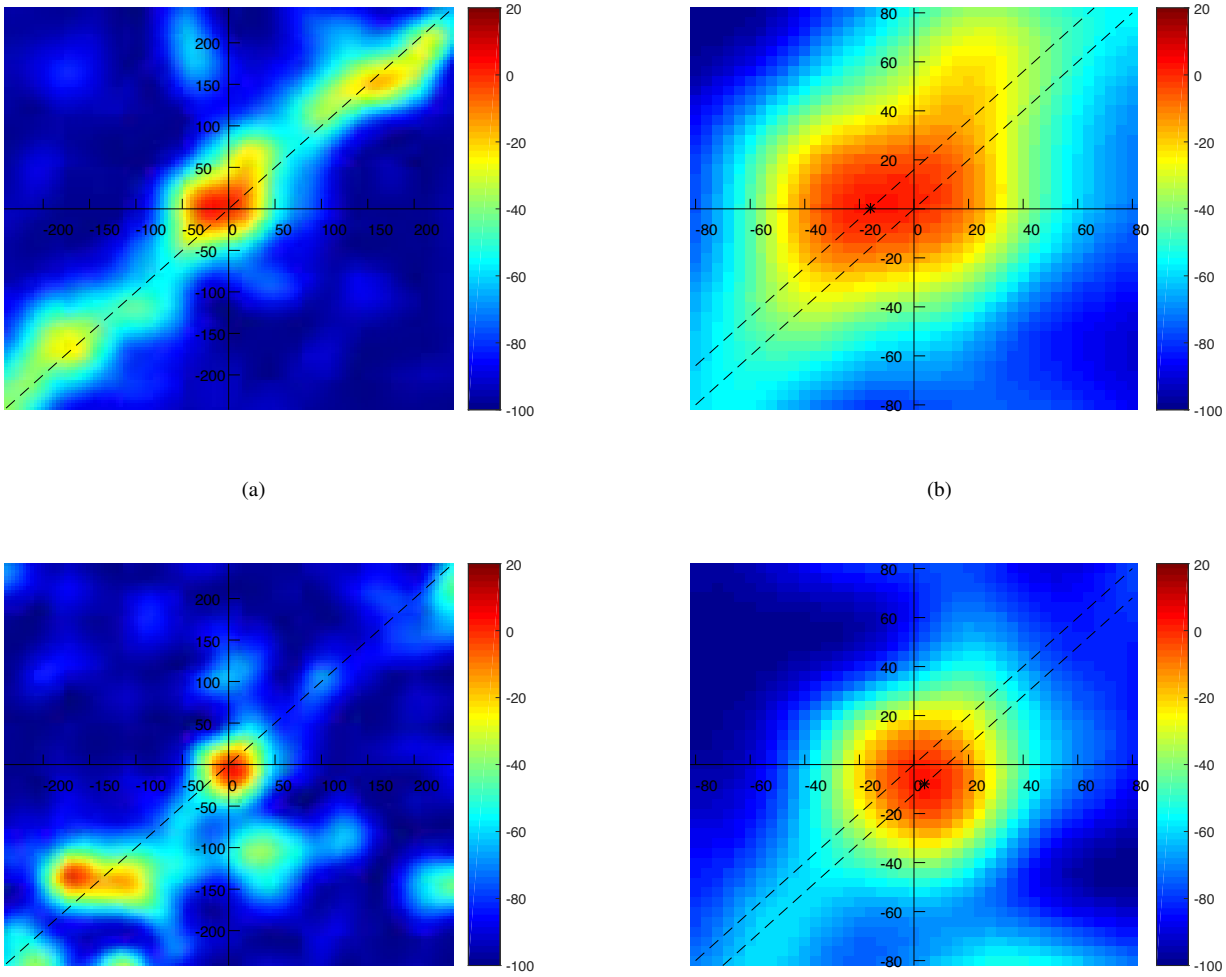

(a) (b) (c) (d)

Fig. 7. Examples of CMCTL and time delay estimation around Peak 1. The *x* axis represents the shift of EEG, while the *y* axis represents the shift of EMG in samples, and the colour represents relative increase of coherence compared with that at the origin $(\tau_1, \tau_2) = (0, 0)$. Plots on the right are zoomed versions of the plots on the left. Local maxima are marked by "$*$" signs. Lines going through the maxima intersect the vertical axis at coordinates which are equal to the delay estimates.

TABLE III
TIME DELAY ESTIMATES OBTAINED BY USING STATE-OF-THE-ART METHODS

Methods	Subject	Time delay (ms) of different time intervals				
		1.5 - 4.5 s	1.5 - 2.5 s	2 - 3 s	2.5 - 3.5 s	3 - 4 s
Phase-based estimation [9]	B	29.76	34.68	34.98	30.73	23.95
	J	1.52	2.07	0.94	2.31	5.69
	K	5.93	2.96	5.16	7.95	12.01
	L	19.17	8.76	28.36	52.59	53.99
	N	-2.71	21.48	14.47	4.38	10.33
Hilbert transform [11]	B	-29.3	-32.23	-31.25	-32.23	-32.23
	J	-16.60	-18.55	-19.53	-18.55	-19.53
	K	11.72	11.72	10.74	9.77	-31.25
	L	-37.11	-40.04	-37.11	-36.13	-39.06
	N	17.58	-51.76	15.63	-55.66	-55.66
Maximising coherence [25]	B	99.61	109.38	-17.58	57.62	28.32
	J	-7.81	-0.94	46.88	30.27	82.03
	K	-26.37	-49.80	0	-10.74	-94.73
	L	-52.73	0	-30.27	89.84	79.10
	N	-118.16	-186.52	21.48	-126.95	75.20

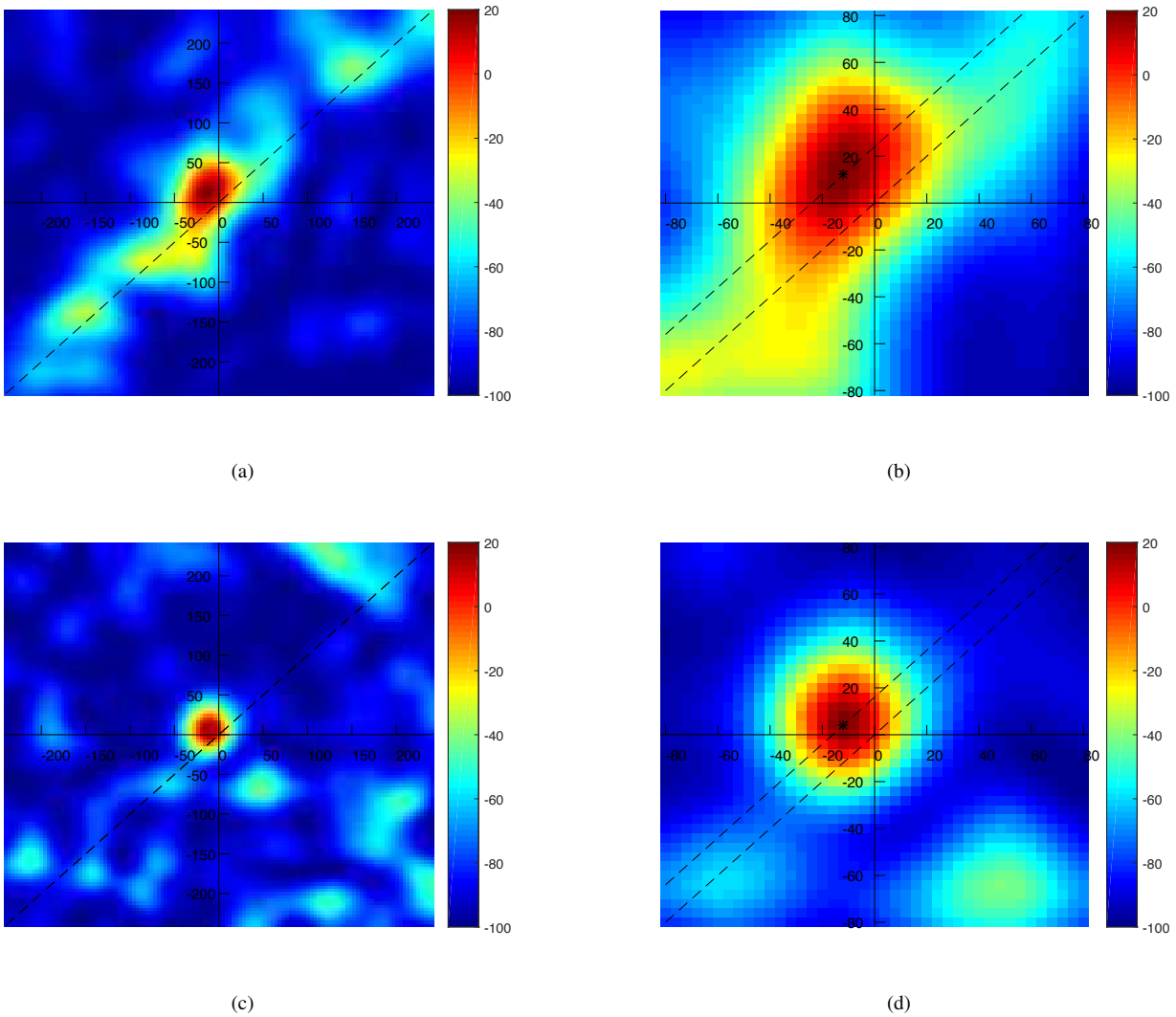

Fig. 8. Examples of CMCTL and time delay estimation around Peak 2. The *x* axis represents the shift of EEG while the *y* axis represents the shift of EMG in samples, and the colour represents relative increase of coherence compared with that at the origin $(\tau_1, \tau_2) = (0, 0)$. Plots on the right are zoomed versions of the plots on the left. Local maxima are marked by "$*$" signs. Lines going through the maxima intersect the vertical axis at coordinates which are equal to the delay estimates.

window function. The shape of the window function, its position in time t_c, and its centre frequency ω_c allow for some level of adaptation that could potentially increase the correlation of $\phi_{t_c,\omega_c}(t)$ with the signal of interest, and/or reduce its correlation with the noise, and thus increase the coherence. Fig. 1(e) shows an example of the opposite effect, where the time-frequency resolution of the spectral analysis at low-frequencies does not match well the synchronised EEG and EMG events, which results in the drop of the coherence below the significance level.

We noticed instances of the CMCTL revealing significant coherence in time-frequency regions where the conventional CMC was not expressed, however, that issue could not be investigated extensively using our data. Three of the subjects recruited for the original study [47] indeed did not express baseline CMC in the β range $(14 - 36$ Hz), which was of primary interest there, however, they all exhibited β-range CMC above the 95% confidence level following the stimulus. Moreover, the spectral analysis using windows of length $T = 125$ ms, performed here, brought the coherence above significance level in some additional regions of the time-frequency plane, where it was not detected in the physiological study for which longer windows, $T = 500$ ms, were used [47].

Fig. 9 illustrates the enhancement of cortico-muscular coherence via a combined effect of adequate time-frequency resolution of the underlying spectral analysis and the CMCTL methodology. While significant coherence in the β range is not expressed in the time interval after 3 s when spectral analysis is performed using Hanning window of length $T = 500$ ms, with $\Delta t = 250$ ms shifts, (see Fig. 9(a)), the plot in Fig. 9(b) shows that the coherence in the same time-frequency region is revealed when Hanning window of length $T = 125$ ms is used, and shifted in time with $\Delta t = 9.8$ ms increments.Then we performed the CMCTL around the peak which emerged at $t_c = 3.461$ s and $\omega_c = 24$ Hz, which increased the level of coherence by another 24%, as shown in Fig. 9(c), bringing

it ultimately to the 0.05 level. It is worth noting also that as a result of employing the time-frequency resolution provided by the shorter window, the coherence is enhanced everywhere in the β range, however it disappeared at frequencies below 10 Hz in the $3-3.5$ s interval, suggesting that optimal time-frequency resolution needs to be non-uniform, and that finding optimal solutions merits further research.

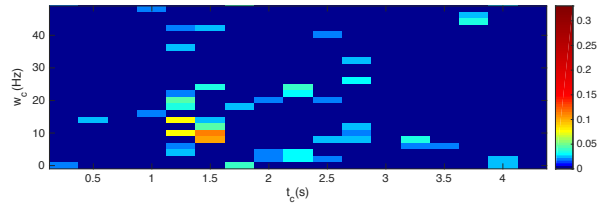

(a)

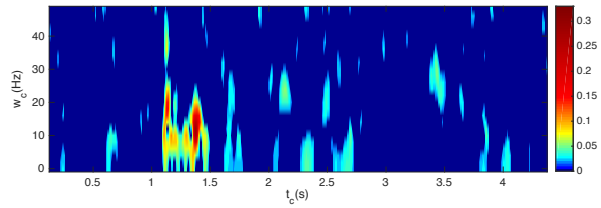

(b)

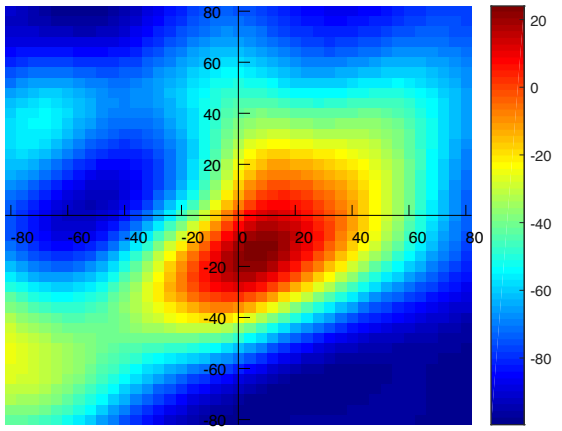

(c)

Fig. 9. Coherence enhancement achieved via adequate time-frequency resolution of spectral estimation combined with CMCTL. (a) The CMC plot obtained via the STFT computed at $M = 512$ frequencies, using Hanning window of length $T = 500$ ms, with $\Delta t = 250$ ms shifts between consecutive windows. The coherence is very weak, and cannot be observed in the β band in the interval after 3 s. (b) The CMC plot obtained via the STFT which is computed using Hanning window of length $T = 125$ ms, with $\Delta t = 9.8$ ms shifts between consecutive windows. The coherence is enhanced almost everywhere in the time-frequency plane, and becomes evident in the β band, in the interval after 3 s. (c) The CMCTL performed around the peak which emerged at $t_c = 3.461$ s, $\omega_c = 24$ Hz. It increases the maximum coherence value by another 24% bringing to 0.05. The colour scale in this plot represents the relative increase of the CTMCTL with respect to the CMCTL at the origin. CMC values below the 95% confidence limit are set to zero in both plots.

V. Conclusion

In this paper we introduced the concept of cortico-muscular coherence with time lag (CMCTL), that is the coherence between EEG and EMG segments taken with a time lag from a central observation point. Using physiological data, we illustrated the potential of the CMCTL function to increase coherence levels and provide information about finer temporal structures of cortico-muscular interactions compared to the conventional cortico-muscular coherence. Then we proposed an algorithm for estimating the delay between coupled cortical and muscular events as the time lag corresponding to local maxima of the CMCTL function, and provided its analysis and interpretation in the context of multi-path propagation, which is a more realistic model of cortico-muscular pathways than the commonly assumed single-path system. Delay estimates obtained by applying the proposed algorithm to physiological data are in close agreement with underlying physiology, whereas in situations when that is not the case, the discrepancies are in agreement with the analysis provided in the paper.

References

[1] Y. Xu *et al.*, "Delay estimation between eeg and emg via coherence with time lag," in *Proc. ICASSP 2016, to be published*.

[2] S. Salenius *et al.*, "Cortical control of human motoneuron firing during isometric contraction," *J. Neurophysiol.*, vol. 77, no. 6, pp. 3401–3405, 1997.

[3] P. Brown *et al.*, "Cortical correlate of the piper rhythm in humans," *J. Neurophysiol.*, vol. 80, no. 6, pp. 2911–2917, 1998.

[4] J. M. Kilner *et al.*, "Human cortical muscle coherence is directly related to specific motor parameters," *J. Neurosci.*, vol. 20, no. 23, pp. 8838–8845, 2000.

[5] J. Groß *et al.*, "Cortico-muscular synchronization during isometric muscle contraction in humans as revealed by magnetoencephalography," *J. Physiol.*, vol. 527, no. 3, pp. 623–631, 2000.

[6] R. Kristeva *et al.*, "Beta-range cortical motor spectral power and corticomuscular coherence as a mechanism for effective corticospinal interaction during steady-state motor output," *Neuroimage*, vol. 36, no. 3, pp. 785–792, 2007.

[7] B. A. Conway *et al.*, "Synchronization between motor cortex and spinal motoneuronal pool during the performance of a maintained motor task in man," *J. Physiol.*, vol. 489, no. Pt 3, pp. 917–924, 1995.

[8] G. C. Carter, "Bias in magnitude-squared coherence estimation due to misalignment," *IEEE Trans. Acoust., Speech, Signal Process.*, vol. 28, no. 1, pp. 97–99, 1980.

[9] T. Mima and M. Hallett, "Electroencephalographic analysis of cortico-muscular coherence: reference effect, volume conduction and generator mechanism," *Clin. Neurophysiol.*, vol. 110, pp. 1892–1899, 1999.

[10] P. Brown *et al.*, "Coherent cortical and muscle discharge in cortical myoclonus," *Brain*, vol. 122, pp. 461–472, 1999.

[11] M. Lindemann *et al.*, "Delay estimation for cortico-peripheral relations," *J. Neurosci. Meth.*, vol. 111, pp. 127–139, 2001.

[12] F. Panzica *et al.*, "Movement-activated myoclonus in genetically defined progressive myoclonic epilepsies: Eeg-emg relationship estimated using autoregressive models," *Clin. Neurophysiol.*, vol. 114, pp. 1041–1052, 2003.

[13] T. Mima *et al.*, "Electroencephalographic measurement of motor cortex control of muscle activity in humans," *Clin. Neurophysiol.*, vol. 111, no. 2, pp. 326–337, 2000.

[14] D. M. Halliday *et al.*, "Using electroencephalography to study functional coupling between cortical activity and electromyograms during voluntary contractions in humans," *Neurosci. Lett.*, vol. 241, no. 1, pp. 5–8, 1998.

[15] C. L. Witham *et al.*, "Contributions of descending and ascending pathways to corticomuscular coherence in humans," *J. Physiol.*, vol. 589, no. 15, pp. 3789–3800, 2011.

[16] M. Pohja and S. Salenius, "Modulation of cortex-muscle oscillatory interaction by ischaemia-induced deafferentation," *Neuroreport*, vol. 14, no. 3, pp. 321–324, 2003.

[17] C. N. Riddle and S. N. Baker, "Manipulation of peripheral neural feedback loops alters human corticomuscular coherence," *J. Physiol.*, vol. 566, no. 2, pp. 625–639, 2005.

[18] M. Cassidy and P. Brown, "Spectral phase estimates in the setting of multidirectional coupling," *J. Neurosci. Meth.*, vol. 127, no. 1, pp. 95–103, 2003.

[19] S. F. Campfens *et al.*, "Face to phase: pitfalls in time delay estimation from coherency phase," *J. Comput. Neurosci.*, vol. 37, no. 1, pp. 1–8, 2014.

[20] S. N. Baker *et al.*, "Afferent encoding of central oscillations in the monkey arm," *J. Neurophysiol.*, vol. 95, no. 6, pp. 3904–3910, 2006.

[21] E. R. Williams *et al.*, "Coherence between motor cortical activity and peripheral discontinuities during slow finger movements," *J. Neurophysiol.*, vol. 102, no. 2, pp. 1296–1309, 2009.

[22] C. L. Witham *et al.*, "Corticomuscular coherence between motor cortex, somatosensory areas and forearm muscles in the monkey," *Front. Syst. Neurosci.*, vol. 4, 2010.

[23] V. M. McClelland *et al.*, "Rectification of the emg is an unnecessary and inappropriate step in the calculation of corticomuscular coherence," *J. Neurosci. Meth.*, vol. 205, no. 1, pp. 190–201, 2012.

[24] G. C. Carter, "Coherence and time delay estimation," *Proc. IEEE*, vol. 75, no. 2, pp. 236–255, 1987.

[25] R. B. Govindan *et al.*, "Estimation of time delay by coherence analysis," *Physica A*, vol. 350, pp. 277–295, 2005.

[26] G. Birò and L. D. Partridge, "Analysis of multiunit spike records." *J. Appl. Physiol.*, vol. 30, no. 4, pp. 521–526, 1971.

[27] J. Weytjens and D. van Steenberghe, "The effects of motor unit synchronization on the power spectrum of the electromyogram," *Biol. Cybern.*, vol. 51, no. 2, pp. 71–77, 1984.

[28] D. F. Stegeman *et al.*, "Surface emg models: properties and applications," *J. Electromyogr. Kines.*, vol. 10, no. 5, pp. 313–326, 2000.

[29] A. Merlo *et al.*, "A fast and reliable technique for muscle activity detection from surface emg signals," *IEEE Trans. Biomed. Eng.*, vol. 50, no. 3, pp. 316–323, 2003.

[30] G. C. Carter *et al.*, "Estimation of the magnitude-squared coherence function via overlapped fast fourier transform processing," *IEEE Trans. Audio Electroacoust.*, vol. 21, no. 4, pp. 337–344, 1973.

[31] Z. Cvetkovic, "On discrete short-time fourier analysis," *IEEE Trans. Signal Process.*, vol. 48, no. 9, pp. 2628–2640, September 2000.

[32] D. R. Brillinger, *Time Series: Data Analysis and Theory*. Siam, 1981, vol. 36.

[33] A. Piersol, "Time delay estimation using phase data," *IEEE Trans. Acoust., Speech, Signal Process.*, vol. 29, no. 3, pp. 471–477, 1981.

[34] M. S. Brandstein and H. F. Silverman, "A robust method for speech signal time-delay estimation in reverberant rooms," in *Proc. ICASSP-97.*, vol. 1, 1997, pp. 375–378.

[35] P. Grosse *et al.*, "Abnormal corticomuscular and intermuscular coupling in high-frequency rhythmic myoclonus," *Brain*, vol. 126, no. 2, pp. 326–342, 2003.

[36] S. Graziadio *et al.*, "Developmental tuning and decay in senescence of oscillations linking the corticospinal system," *J. Neurosci.*, vol. 30, no. 10, pp. 3663–3674, 2010.

[37] D. Farina *et al.*, "The extraction of neural strategies from the surface emg," *J. Appl. Physiol.*, vol. 96, no. 4, pp. 1486–1495, 2004.

[38] K. G. Keenan *et al.*, "Influence of amplitude cancellation on the simulated surface electromyogram," *J. Appl. Physiol.*, vol. 98, no. 1, pp. 120–131, 2005.

[39] R. HODES *et al.*, "The human electromyogram in response to nerve stimulation and the conduction velocity of motor axons: studies on normal and on injured peripheral nerves," *Arch. Neuro. Psychiatr.*, vol. 60, no. 4, pp. 340–365, 1948.

[40] M. Vecchierini-Blineau and P. Guiheneuc, "Electrophysiological study of the peripheral nervous system in children. changes in proximal and distal conduction velocities from birth to age 5 years." *J. Neurol. Neurosur. Ps.*, vol. 42, no. 8, pp. 753–759, 1979.

[41] G. J. Parry *et al.*, *Guillain-Barre Syndrome: From Diagnosis to Recover*. Demos Medical Publishing, 2007.

[42] N. Hogan and R. W. Mann, "Myoelectric signal processing: Optimal estimation applied to electromyography - part i: Derivation of the optimal myoprocessor," *IEEE Trans. Biomed. Eng.*, vol. BME-27, no. 7, pp. 382–395, July 1980.

[43] ——, "Myoelectric signal processing: Optimal estimation applied to electromyography - part ii: Experimental demonstration of optimal myoprocessor performance," *IEEE Trans. Biomed. Eng.*, vol. BME-27, no. 7, pp. 396–410, July 1980.

[44] P. Parker *et al.*, "Signal processing for the multistate myoelectric channel," *Proc. IEEE*, vol. 65, no. 5, pp. 662–674, May 1977.

[45] E. Clancy and N. Hogan, "Single site electromyograph amplitude estimation," *IEEE Trans. Biomed. Eng.*, vol. 41, no. 2, pp. 159–167, Feb 1994.

[46] ——, "Probability density of the surface electromyogram and its relation to amplitude detectors," *IEEE Trans. Biomed. Eng.*, vol. 46, no. 6, pp. 730–739, June 1999.

[47] V. M. McClelland *et al.*, "Modulation of corticomuscular coherence by peripheral stimuli," *Exp. Brain Res.*, vol. 219, no. 2, pp. 275–292, 2012.

[48] A. Siegel and H. N. Sapru, *Essential Neuroscience*. Lippincott Williams & Wilkins, 2006.

Yuhang Xu received the B.Eng. degree in Electronic Information Engineering and M.Eng. in Circuits and Systems from Chongqing University, Chongqing, China, in 2010 and 2013, respectively.

She is currently a Ph.D. student in the Department of Informatics, King's College London. Her research interests include signal processing methods in neuroscience.

Verity M. McClelland obtained her PhD from the University of Newcastle upon Tyne in 1999, investigating descending modulation of upper limb reflex patterns in healthy humans, adults with stroke and children with cerebral palsy. She continued training in clinical Paediatric Neurology, including at St. Thomas' Hospital, London and was awarded an NIHR Academic Clinical Lectureship in Clinical Neurophysiology at the Institute of Psychiatry, Psychology and Neuroscience, Kings College London, from 2008-2016. She currently works as a locum consultant in Clinical Neurophysiology at Great Ormond Street Hospital for Children, London and she has recently been awarded a Post-doctoral Clinical Research Training Fellowship from the Medical Research Council to further investigate sensory abnormalities in childhood dystonia.

Zoran Cvetković (SM'04) is Professor of Signal Processing at Kings College London. He received his Dipl. Ing. and Mag. degrees from the University of Belgrade, Yugoslavia, the M.Phil. from Columbia University, and the Ph.D. in electrical engineering from the University of California, Berkeley. He held research positions at EPFL, Lausanne, Switzerland (1996), and at Harvard University (2002-04). Between 1997 and 2002, he was a Member of the Technical Staff of AT&T Shannon Laboratory. His research interests are in the broad area of signal processing, ranging from theoretical aspects of signal analysis to applications in audio and speech technology, and neuroscience. From 2005 to 2008, he served as an Associate Editor of IEEE TRANSACTIONS ON SIGNAL PROCESSING.

Kerry R. Mills was trained at Kings College Hospital and qualified in Medicine in 1975 after having completed a PhD in Neurophysiology and having worked as a Lecturer in Physiology at Kings College London. After junior training posts and research posts at University College Hospital and The National Hospital, Queen Square, he went to Oxford as a University Lecturer in Clinical Neurophysiology in 1987 and was awarded a personal chair in 1998. In 1999 he moved to his current position as Professor of Clinical Neurophysiology, University of London, Kings College. His research interests include muscle disease, muscle fatigue, motor control and the use of transcranial magnetic stimulation to investigate corticospinal function in health and disease.